PAPER

Effects of optical diagnostic techniques on the accuracy of laminar flame speeds measured from Bunsen flames: OH* chemiluminescence, OH-PLIF and acetone/kerosene-PLIF

View the article online for updates and enhancements.

Effects of optical diagnostic techniques on the accuracy of laminar flame speeds measured from Bunsen flames: OH* chemiluminescence, OH-PLIF and acetone/kerosene-PLIF

Yi Wu[1,2] ⓘ**, Vincent Modica**[2]**, Xilong Yu**[1,3]**, Fei Li**[1] **and Frédéric Grisch**[2]

[1] State Key Laboratory of High Temperature Gas Dynamics, Institute of Mechanics, Chinese Academy of Sciences, Beijing 100190, People's Republic of China
[2] CORIA—UMR 6614, Normandie Université, CNRS, INSA et Université de Rouen, Campus Universitaire du Madrillet, 76800 Saint-Etienne du Rouvray, France
[3] School of Engineering Science, University of Chinese Academy of Sciences, Beijing 100049, People's Republic of China

E-mail: yi.wu@imech.ac.cn

Abstract

The effects of optical diagnostic techniques on the accuracy of laminar flame speed measured from Bunsen flames were investigated. Laminar flame speed measurements were conducted for different fuel/air mixtures including CH_4/air, acetone/air and kerosene (Jet A-1)/air in applying different optical diagnostic techniques, i.e. OH* chemiluminescence, OH-PLIF and acetone/kerosene-PLIF. It is found that the OH* chemiluminescence imaging technique cannot directly derive the location of the outer edge of the fresh gases and it is necessary to correct the position of the OH* peak to guarantee the accuracy of the measurements. OH-PLIF and acetone/kerosene-PLIF respectively are able to measure the disappearance of the fresh gas contour and the appearance of the reaction zone. It shows that the aromatic-PLIF technique gives similar laminar flame speed values when compared with those obtained from corrected OH* chemiluminescence images. However, discrepancies were observed between the OH-PLIF and the aromatic-PLIF techniques, in that OH-PLIF slightly underestimates laminar flame speeds by up to 5%. The difference between the flame contours obtained from different optical techniques are further analysed and illustrated with 1D flame structure simulation using detailed kinetic mechanisms.

Keywords: OH* chemiluminescence, OH-PLIF, acetone-PLIF, kerosene-PLIF, laminar flame speed

(Some figures may appear in colour only in the online journal)

1. Introduction

Laminar flame speed S_L is an important parameter in studying the combustion process, and it contains fundamental information on the diffusivity, reactivity and exothermicity of combustible mixtures. Accurate experimental measurements of laminar flame speed can be used to validate newly developed chemical kinetic mechanisms, as well as turbulence combustion models [1]. In order to be useful in restraining the uncertainty of chemical models, the accuracy of laminar flame speed measurements is extremely important due to the low sensitivity of S_L to kinetic mechanisms. Recently, substantial

attention has been paid to the accuracy of flame speed measurements by taking a comprehensive account of different sources of uncertainty, such as mixture preparation, ignition, flame instability, radiation and linear or nonlinear stretch behaviour for different flame configurations [2]. Despite the fact that considerable effort has been devoted to understanding the sophistications and physics behind each approach, accurate flame speed measurement is still an open issue, especially for large molecular weight fuels generally present in practical fuels such as gasoline, diesel and kerosene utilized in automobile and aeronautic engines [3].

Laminar flame speed is defined by the velocity at which a laminar, steady, plane, un-stretched, adiabatic flame freely propagates relative to the unburned premixed gas in the direction normal to the flame surface [4]. Among the various experimental methodologies developed to measure this parameter [1, 5–7], the Bunsen flame method is one of the most utilized approaches due to the simplicity of its experimental arrangements and its well-defined flame structure [8, 9]. For a conical flame stabilized on a nozzle, assuming that the laminar flame speed is the same across the whole flame surface, the flame speed can be derived by applying mass conservation law between the nozzle outlet and flame front, and it is expressed by $S_L = Q_m/\rho_u A$. Since the layer of interest is on the unburned side of the flame, ρ_u will be the density of the unburned gas and Q_m/ρ_u will be close to the volume flowrate of the unburned gas. Hence, to obtain a value for flame speeds in practice, by taking fresh gases into account, it is necessary to locate and measure a flame area A as close to the unburned side of the flame as possible. Even though the aforementioned definition of laminar flame speed is simple and without ambiguity, optical diagnostic techniques currently being applied to extract fresh gases from the front of a conical flame are still inadequate to produce very accurate measurements of laminar flame speed. This flame front, corresponding to the unburned gases close to the reaction zone, is not easily measurable due to the asymptotic nature of the temperature profile.

A review of the literature reveals that various optical methods for locating the position of the flame front have been proposed and used in the past to measure laminar flame speed. These mainly include flame emission imaging techniques, i.e. chemiluminescence, the Shadowgraph/Schlieren image technique and the OH-PLIF techniques [10–12].

Flame emission imaging techniques (i.e. usually OH* chemiluminescence) consist of recording the spatial distribution of the flame front emission [13, 14]. Generally for hydrocarbon/air mixtures, the signal emitted by the flame is sufficiently luminous to satisfactorily describe the flame contours, and so it has been frequently used to measure laminar flame speeds [8]. However, the luminous zone, representing the zone of the reactive species, is located some distance behind the initial temperature rise, which is different to the preheating zone. This surface would therefore appear to be unsuitable for directly determining flame speed unless an estimation of the flame thickness (δ) can be determined [8]. The shadow graphic technique measures the derivative of density gradient, which is the result of refraction index variation across the flame front [15]. Past experiments have revealed that the
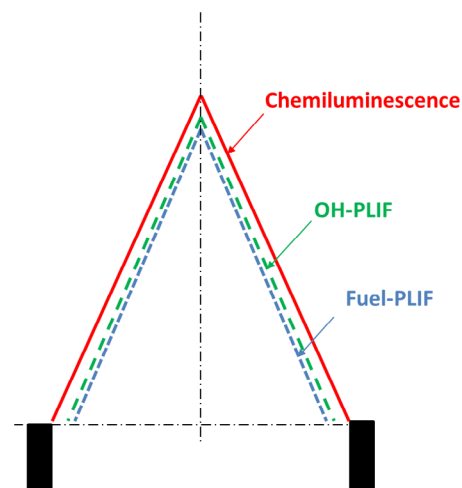
Figure 1. Schematic of flame contours using OH*-chemiluminescence, OH-PLIF and Fuel-PLIF techniques.

sharp inner shadow graphic edge is dependent on the distance between the flame and the optical detector [16]. Suitable correction needs to be performed to ensure the accuracy of measurements, meaning that this technique has seldom been used in laminar flame speed measurements. Another drawback of these techniques is their line-of-sight nature, i.e. the signal obtained is an averaged value over the volume of the flame as a whole, leading to an ambiguity of the local 2D flame structure. More recently, advanced laser diagnostic techniques such as planar laser-induced fluorescence have been implemented in the measurement of laminar flame speed based on the Bunsen flame approach [8, 9]. The excitation of radicals, such as hydroxyl radicals OH, became a standard procedure within combustion laser diagnostics, and this technique has been widely applied in flame front detection [12, 17, 18]. Another possible optical diagnostic technique that can be used in laminar flame speed is Fuel-PLIF (i.e. the acetone/kerosene planar-induced fluorescence imaging technique [19, 20] in the present work). By collecting the fluorescence intensity emitted by the fuel, Fuel-PLIF can directly visualize the fresh gas contours, providing a potential alternative solution for accurate laminar flame speed measurements. A schematic of the different flame contours visualized by the aforementioned optical techniques is shown in figure 1. As illustrated in this figure, the different locations of the flame front will subsequently introduce considerable discrepancies in flame speed determination, and so this has to be quantitatively investigated.

In the present work, the effect of these different optical diagnostic techniques on the accuracy of flame speed measurements based on the Bunsen flame approach will be quantitatively elucidated. The popular OH* chemiluminescence and OH-PLIF optical diagnostic techniques will be revisited using different reactive mixtures: CH4/air, acetone/air and kerosene (Jet A-1)/air. In this work, the raw OH* chemiluminescence signals will be corrected using flame thicknesses calculated from simulations. Indeed, the progress of numerical tools and more robust kinetic mechanisms enable us to accurately calculate theoretical flame thicknesses and to better correct the determination of Bunsen flame area (by considering the
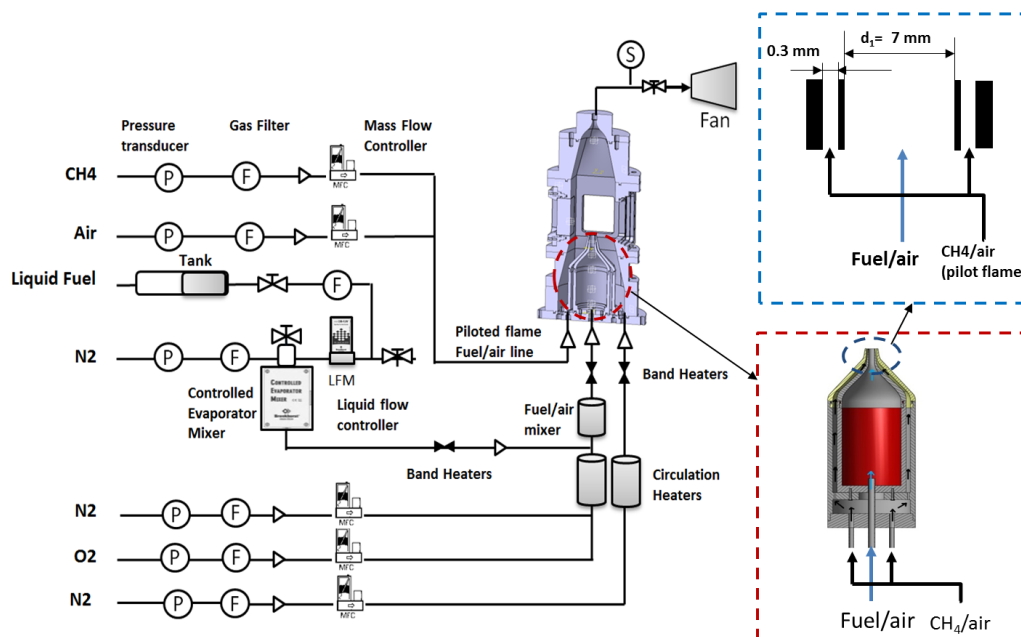
Figure 2. Experimental set-up.

fresh gases side) [8]. Additionally, in order to generalize the OH* chemiluminescence technique to fuel/air mixtures whose kinetic mechanisms are less available, a new image processing methodology is proposed, which allows the fresh gas contours from OH* chemiluminescence imaging to be relocated. Finally, the PLIF technique will be extended to self-fluorescing hydrocarbon fuels, i.e. acetone-PLIF [19] and kerosene-PLIF techniques [20], providing a potential alternative solution for detecting accurate fresh gas contours in laminar flame speed measurements.

As previously presented in [8], the experimental system and the image processing algorithm have been validated by laminar flame speed measurements for CH4/air mixture, which is one of the most studied fuels in the literature. Details of the experimental method can be found in [8]. In the present work, a new comparison of flame speed data is added in order to accurately assess different post-treatment methods. Then, Bunsen flames of acetone/air mixture are studied because the acetone molecule is a convenient fluorescence tracer which has been extensively used in the acetone-PLIF technique for flow visualization and combustion studies. This is due to its photo-physical advantages and because its detailed kinetic mechanism (Chong *et al* [21]) has been well-developed and validated by various previous works, enabling us to accurately compare the fuel-PLIF technique with the simulation results. Finally, laminar flame speed measurements of the kerosene/air mixture are subsequently performed using these three optical techniques, i.e. the OH* chemiluminescence, OH-PLIF and fuel-PLIF techniques. These parts of the results are compared with the simulation results obtained by using the skeletal kerosene mechanism (LUCHE mechanism [22]). Comparisons and a discussion of these three optical techniques for measuring laminar flame speed are finally performed in the discussion section.

2. Experimental setup and procedures

2.1. Bunsen flame burner

In this study, laminar flame speeds were measured using a Bunsen flame burner in a closed chamber. The premixed Bunsen flame burner allows for the establishment of a steady conical laminar premixed flame stabilized on the outlet of a contoured nozzle. The contoured nozzle used in the present work has an outlet diameter $d_1 = 7$ mm. A concentric contoured nozzle with an outlet diameter of $d_2 = 7.6$ mm surrounding the central nozzle is used to produce a pilot flame (CH$_4$/air) to stabilize the flame in equivalence ration extreme conditions. As illustrated in figure 2, the whole burner is placed into a N$_2$ ventilated chamber constructed in stainless steel, with an inner surface of 100×100 mm^2 and a height of 511 mm. Five type K thermocouples are placed at different positions in the chamber to monitor and ensure uniformity throughout the chamber. The valve located after the chamber is fully opened to guarantee atmospheric pressure conditions. With four large UV quartz windows, it is accessible in order that the flame can be probed using optical imaging diagnostics.

The burner can operate with gaseous or liquid fuels. The liquid fuels, pressurized in a 1.0 l tank, were delivered by a liquid flow controller (Bronkhorst mini CORI-FLOW) to a controlled evaporator and mixer (CEM, Bronkhorst), which heats and mixes the fuel vapour with N$_2$ carrier gas at a controlled mass flow rate and temperature. Additional nitrogen and oxygen, controlled by two mass flow controllers (MFC), are mixed and used to reproduce the synthetic species composition of air and to modify the equivalence ratio of the heated fuel vapour/air mixtures. To prevent any condensation of the fuel vapour, the reactive mixture and the guard flow are preheated with two circulation heaters before entering the mixing
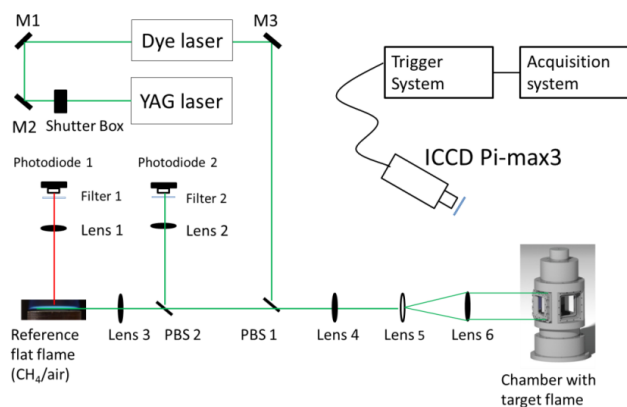
Figure 3. Diagnostic arrangements.

Figure 4. Excitation fluorescence spectrum of the OH radical recorded in the reference flame.

cell and the chamber and gas feeding lines are preheated using an electrical wire heater wrapped around its external surface. Finally, the combustion products are evacuated and cooled through rigid stainless steel tubing connected to the top of the chamber.

2.2. Optical diagnostics

2.2.1. OH* chemiluminescence.
The first optical technique used in the current study is based on the detection of the flame contour with the OH* chemiluminescence optical imaging technique. The camera used to record the OH* radical emission is a thermoelectrically cooled, 16-bit intensified CCD camera (Roper Scientific) with a 1024×1024 array. The camera is equipped with an *f*/2.8, $f = 100$ mm, achromatic UV lens (CERCO) combined with an interference bandpass filter centred at 310 nm and with a bandwidth of 10 nm. The exposure time selected to record the OH* emission image is defined by opening the intensifier gate at 1 μs. A 40×40 mm^2 area of the flame is imaged by the ICCD camera, so that the spatial resolution is about 40 μm per pixel. The acquisition repetition rate of the camera is kept at 10 Hz.

2.2.2. OH-PLIF.
The OH planar laser-induced fluorescence laser diagnostic (OH-PLIF) consists of a cluster system, which includes an Nd:YAG laser, a dye laser, a calibration system and a high-resolution ICCD camera. A frequency-doubled, *Q*-switched Nd: YAG laser was used to pump a dye laser, which was then frequency-doubled to obtain wavelengths in the 280–290 nm spectral range. The UV laser beam was tuned to 282.75 nm to excite the Q1(5) line of the (1, 0) vibrational band of the OH ($X^2\Pi - A^2 \sum^+$) system. The laser energy was fixed at 5 mJ to maintain the fluorescence of OH radical within the linear regime, maintaining the proportionality between the OH fluorescence signal and the OH concentration. As illustrated in figure 3, the UV beam is initially split into two parts at the exit of the laser source by a plane UV window (PBS 1). **(a)** The function of the 4% reflected laser beam is to tune the laser wavelength to the line-centre of the OH transition. To do this, a second plane UV window (PBS-2) enables 4% of the reflected UV beam to be taken out again, in order to control the laser energy in time using a fast UV photodiode. The resulting transmitted UV beam then enables
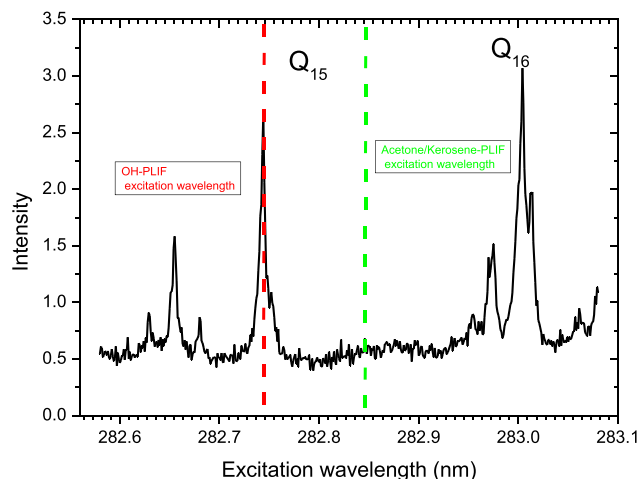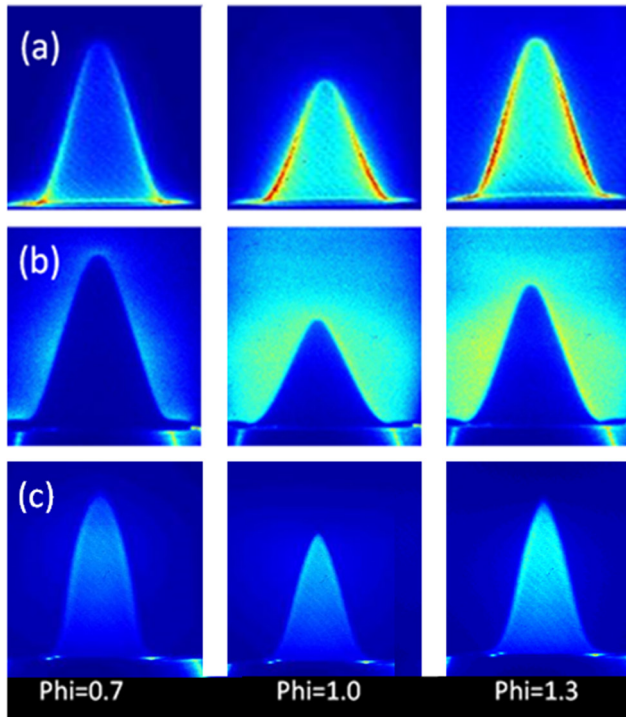
the excitation of the OH radical produced in a reference flame. The premixed flame is generated via a porous burner fed with a methane/air mixture. The OH fluorescence is collected at a right angle with a UV photomultiplier (PMT). The signal collected from the PMT is then amplified by a high-current amplifier to deliver a 0–10 V DC signal. **(b)** The remaining UV laser beam after the first plane UV window is formed into a collimated laser sheet using two cylindrical lenses and one spherical lens. The cylindrical lenses, 50 mm and 300 mm in focal length, form a cylindrical telescope which spreads the beam into a collimated, sheet of 5 cm tall. The spherical lens, 1 m in focal length, focuses the sheet to a 150 μm waist. The laser sheet is then oriented inside the combustion chamber to excite the OH radical.

The spatial distribution of the OH fluorescence in the flame is recorded on the ICCD camera (the same one used for the OH* chemiluminescence technique). The intensifier gate width is set to 1 μs and the framing rate of the acquisition of fluorescence images is 10 Hz. The camera is equipped with the same optical lens and optical filters as for the OH* chemiluminescence diagnostic. Finally, the sensing instrumentation (ICCD camera, PMT and fast UV photodiodes) is interfaced to a PC computer, which is used to control the camera and acquire the experimental signals via a LABVIEW program.

2.2.3. Acetone/kerosene-PLIF.
The acetone/kerosene planar-induced fluorescence imaging technique offers the advantage of easily imaging the frontiers of fuel consumption inside the flame. In the current work, the laser excitation of acetone is performed by the laser source used for the OH-PLIF diagnostic. As acetone displays a broadband absorption spectrum extending from 230 to 320 nm, the excitation wavelength of acetone can be fixed to any convenient wavelength located within this domain. However, for a flame, the excitation wavelength of acetone must be selected to ensure that this wavelength is far from the resonance of an OH transition. Figure 4 displays a portion of the OH fluorescence spectrum recorded within the 282.65–282.90 nm spectral domain coming from the reference flame. As observed in this fluorescence spectrum, the OH transition, i.e. the Q1(5) and Q1(6) rotational
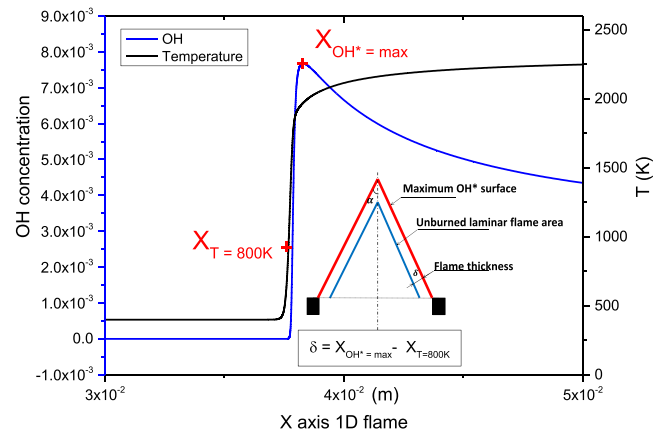
Figure 6. OH and temperature profiles from 1D flame simulation and flame thickness determination with the CH4/air mixture ($T = 300\,\mathrm{K}$, $\varphi = 1$ and $P = 0.1\,\mathrm{MPa}$).

Figure 5. Acetone/air flames for various equivalence ratios $\varphi = 0.7$, 1.0 and 1.3: (a) OH* chemiluminescence images; (b) OH-PLIF images; (c) acetone-PLIF images.

lines, are well-separated, giving the opportunity to tune the excitation wavelength of acetone at 282.85 nm in a spectral region in which only the collection of acetone fluorescence will be permitted. Acetone fluorescence was then acquired by illuminating the acetone/air flame with the same optical arrangement as that used for the OH-PLIF technique. Only the spectral optical filers placed in front of the ICCD camera were changed, in order to collect the whole broadband fluorescence spectrum of acetone (i.e. between 300–550 nm).

Similar to the acetone-PLIF optical diagnostic, kerosene fuels (Jet A-1, for instance) also have the advantage of issuing a broadband fluorescence emission covering the 260–420 nm spectral domains. This fluorescence emission arises from the excitation of aromatics (i.e. mono- and di-aromatics) naturally present in the chemical composition of these multi-component fuels. Aromatics may be excited on the same wavelength as that used for acetone, and as they are consumed with the fuel at the flame front, they can be used to image the unburned regions of the combustion volume. In the current work, fluorescence images of aromatics were acquired by illuminating the kerosene/air flames with the same optical arrangement as that used for the acetone-PLIF technique. An example image of a flame with the acetone/air mixture using these three different optical diagnostic techniques is illustrated in figure 5.

2.3. Measurement uncertainties

For each measurement condition reported in this work, 30 instantaneous images are systematically recorded and the resulting laminar flame speed is determined by data processing an averaged image deduced from this set of instantaneous
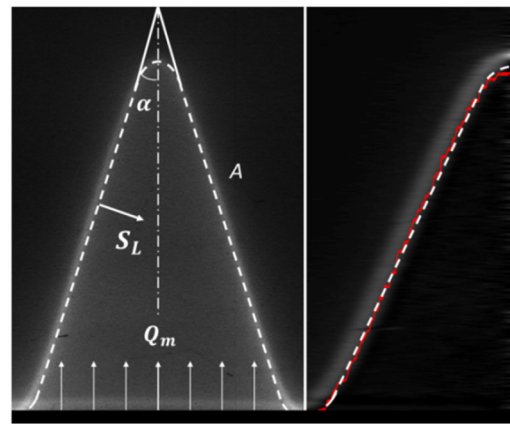

Figure 7. Determination of fresh gas flame surface area by imaging processing (a) original OH* chemiluminescence image; (b) left half of image with Abel inversion (red line is the original curve found by taking the inside front of the image with Abel inversion, dash line is the line used for calculating flame speed obtained after smoothing function).

images. The main source of measurement errors comes from the gas/liquid flow delivery system (U_{Q_m}) and uncertainty regarding the calculated flame area image (U_A), which is determined by the camera resolution. The uncertainty of the total flow rate comes from uncertainty regarding the mass flow controller (0.5% of the reading + 0.1% full scale) which is estimated to be ~2%, and uncertainty deriving from the camera's spatial resolution, which is estimated to be ~3%. The overall uncertainty is calculated to be within 4% (from the relation $\sqrt{U_{Q_m}^2 + U_A^2}$) for all of the laminar flame speeds presented in this work.

3. Determination of laminar flame speed

3.1. OH* chemiluminescence image processing

As previously mentioned, the definition of laminar flame speed is referenced as the preheat zone of fresh gas, which is different from the chemiluminescence luminous zone. Accordingly, the flame surface area used for determining flame speed in the
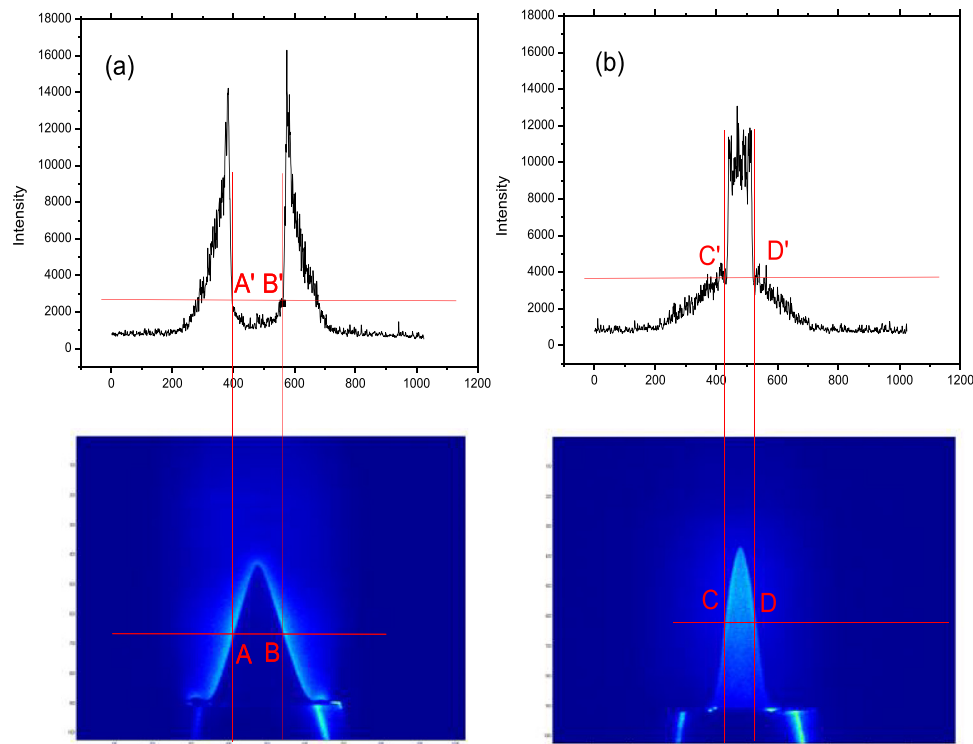
Figure 8. Illustration of the image processing of (a) OH-PLIF and (b) acetone/aromatics-PLIF techniques.

equation $S_L = Q_m/\rho_u A$ from OH* chemiluminescence can be obtained by shifting the maximum intensity contours with a flame thickness in the direction to fresh gas. This flame thickness can be obtained in the present work either by accurately simulating a 1D adiabatic premixed flame or by image processing estimation [8, 23]. For fuel/air mixtures whose detailed chemical kinetic mechanisms have been relatively well developed, such as CH_4/air and acetone/air mixtures, this flame thickness is calculated by simulating a 1D adiabatic premixed flame with Cosilab software. With the OH and temperature profiles obtained from 1D flame simulation, the theoretical 'flame thickness' is calculated as the distance separating the isotherm $T = 800\,K$, in which OH begins to be experimentally detected using optical diagnostics, and the frontier with maximum theoretical OH concentration (figure 6).

For fuel/air mixtures with a less available detailed kinetic mechanism, such as kerosene/air mixtures, the flame contours are obtained through image processing. In this case, a MATLAB program is developed in the present work to perform the Abel inversion of the recorded images, in order to provide the 2D boundary of the surface area at the reaction zone of the flame [24]. The flame front used to calculate surface A is then obtained by taking the inside boundary of the surface area from the image after Abel inversion (figure 7). Once the flame front is determined, the flame area A is calculated by pivoting this flame front profile $f(x)$ along the burner axis using the following equation:

$$A = 2\pi \int_a^b f(x)\sqrt{1 + |f'(x)|^2}\,dx$$

where a and b are the boundary limits of integration and $f(x)$ is the flame contour profile function obtained through image processing.

3.2. OH-PLIF/acetone/kerosene-PLIF image processing

Compared to the processing procedures for OH* chemiluminescence imaging, the data processing of OH/acetone/kerosene-PLIF is largely simplified. The inner contour delimiting the region of OH-fluorescence on the fresh gases side is determined by considering the first pixel in which OH fluorescence appears (figure 8(a)).

For organic tracers such as acetone and aromatics, the data processing of the image is similar to the preceding one. The outer edge of the fresh gases is defined as the position at which the fluorescence of the organic tracer disappears (figure 8(b)). As with OH, this location corresponds to the frontier delimiting a chemical transformation of these organic molecules through the action of chemical reactions. Typically, these organic molecules disappear when OH starts to be optically detected.

It should be noted that in the current work, the laminar flame speeds measured are strictly S_L since stretch effects are not taken into account as compared to the un-stretched flame speed S_L^0. The stretch effect mainly comes from the curvature part located at the tip of the flame. Fortunately, in the present work as the geometry of the nozzle was designed to minimize the boundary layer thicknesses, the velocity profile at the nozzle exit is flat enough that the stretch effect can be negligible [25].
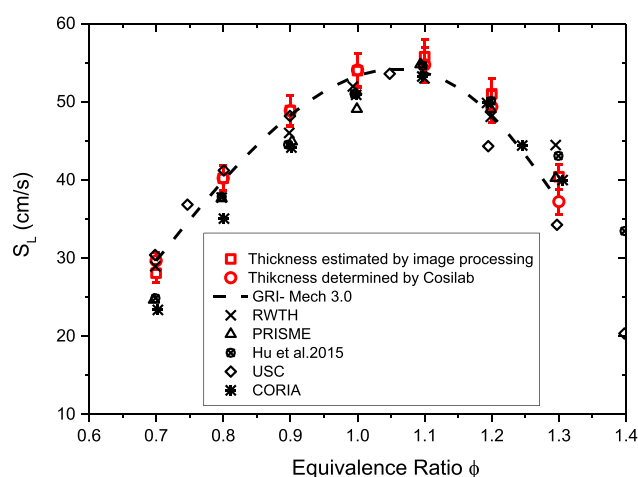
Figure 9. Laminar flame speed comparison between experiments and simulation results using CH$_4$/air $T = 373$ K, $P = 0.1$ MPa and $\varphi = 0.7$–1.3.

Figure 10. Laminar flame speed of acetone/N$_2$/O$_2$ mixtures measured by the OH-PLIF and acetone-PLIF techniques at $T = 443$ K, $P = 0.1$ MPa, $\varphi = 0.7$–1.3.

4. Results and discussion

4.1. Flame thickness correction for OH* chemiluminescence

In order to validate the whole experimental system and to investigate the accuracy of the OH* chemiluminescence technique, preliminary measurements are firstly conducted with CH$_4$/air mixtures using the OH* chemiluminescence technique. As previously discussed, when the chemiluminescence technique is applied, specific flame thickness corrections need to be considered. Hereby, the 'flame thickness' when using CH$_4$/air is obtained by both digital simulation using GRI-Mech 3.0 [26] and by the aforementioned image processing method. Figure 9 depicts the laminar flame speed of CH$_4$/air mixtures obtained by using both of the two strategies at conditions of $T = 373$ K, $P = 0.1$ MPa and $\varphi = 0.6$–1.3. The results of the present work are compared with experimental results found in the literature and numerical results using GRI-Mech 3.0. An observation of the results reveals that both strategies are in good agreement with the simulation results from the GRI-Mech 3.0 mechanism. There are tiny differences between both methods, especially on the equivalence ratio lean side $\varphi = 0.7$–1.2; however the discrepancy begins to amplify on the fuel rich side $\varphi = 1.2$–1.3 up to 3 cm s^{-1}. This could be caused by the flame instability in fuel rich side conditions; if the flame flickers, it leads to larger uncertainty in terms of image processing procedures. Compared to the results from the literature, the data from the present work show good agreement with data from different groups using the constant volume bomb (CORIA, PRISME and RWTH [27]) for the mixture of fuel lean ($\varphi = 0.7$) conditions. Meanwhile, measurements from Hu *et al*'s [28] group are larger than the present measurement on the fuel lean side and agree better on the fuel rich side. From conditions $\varphi = 1.0 - 1.3$, our results are slightly higher compared with other experimental results; meanwhile they have a good accordance with GRI-Mech 3.0 simulation results.

The preliminary results have shown the high ability of OH* chemiluminescence images post-processing (corrected by
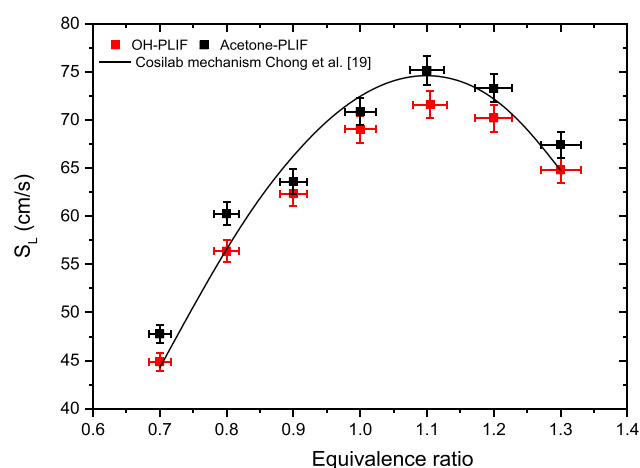
flame thickness) to determine laminar flame speed with reasonable accuracy, similar to those encountered for spherical expanding flames. Moreover, the above analysis concludes that both strategies (i.e. flame thickness estimated both by image processing and determined by simulation) give reasonable laminar flame speed results. However, it should be noted that flame thickness determined by simulation can only be applied when robust detailed kinetic mechanisms are available. In the case of fuels with a complex composition and without very robust kinetic mechanisms, the image processing method is preferable when it comes to estimating flame thickness, as we will see in the next part of this work. For this method, the stability of the Bunsen flame will be a key issue.

4.2. OH/fuel laser-induced fluorescence

In this section, the experimental results for the acetone/air and kerosene/air mixtures, obtained by OH-PLIF and fuel-PLIF, will be discussed.

4.2.1. Acetone/air mixtures. Laminar flame speed results are firstly presented for the acetone/air mixture in order to compare the OH-PLIF and fuel-PLIF methodologies. The experimental data are also compared with the simulation results from Chong *et al*'s mechanism [21]. To the author's knowledge, no experimental data for determining acetone laminar flame speed are available in the literature under these conditions. Figure 10 describes the evolution of the laminar flame speeds of acetone/air mixtures determined from the OH-PLIF and fuel-PLIF techniques in function of their equivalence ratio. Results of the simulation obtained by using Chong *et al*'s mechanism [21] are also plotted in the figure. For each set of equivalence ratio conditions, differences (up to 2–4 cm s^{-1}) between the resulting laminar flame speeds are observed. The laminar flame speeds derived from the acetone-PLIF technique are in good accordance with those deduced from the simulation. Depending on the equivalence ratio, however, slight differences are noted but these are comparable to the uncertainty of our experiments, which is around 4%
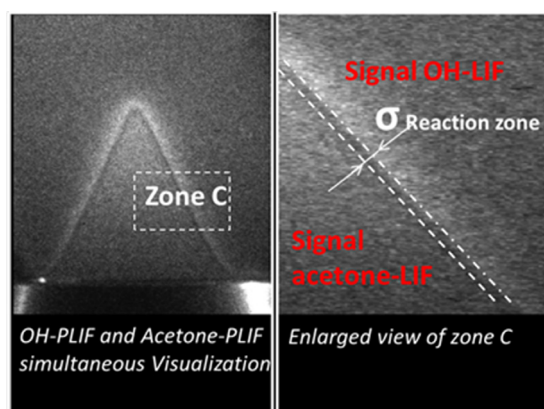
Figure 11. Simultaneous visualization of OH-PLIF and acetone-PLIF images.

and comes from the uncertainty caused by flow meters and camera resolution.

However, considerable differences between the OH-PLIF and acetone-PLIF measurements are observed, especially for equivalence ratios approaching stoichiometry conditions. To explain the differences between laminar flame speeds, figure 11 shows a typical example of OH and acetone-PLIF images acquired simultaneously. An examination of this fluorescence image reveals that the acetone consumption frontier does not coincide with the OH detection frontier. We observed a thin opaque zone between both frontiers in which fluorescence signals are not detected (see enlarged view of zone C in figure 11. One probable reason that may explain such behaviour relates to the dynamics of the ICCD camera used to record our fluorescence signals. In a flame front with high concentration and temperature gradients, the OH concentration can vary by a distance of several hundred μm from 0 to about 1%. With a 'classical' dynamics of 16 bit which is the full dynamic available for an ICCD camera, and assuming a peak OH concentration of about 1% after the flame front, the minimal OH concentration detectable by the ICCD camera will be then close to a few dozen ppm. Unfortunately, this level of concentration is well above the expected OH concentration produced (few ppm) at the inner frontier of the flame front, significantly hindering the early detection of this frontier and so leading to a possible bias in laminar flame speed measurements. The same type of analysis can also be applied to the acetone-PLIF technique. However, in that case, a reduction of the acetone fluorescence signal due to chemical reactivity is easier to detect on the fluorescence image because the acetone fluorescence signal inside the fresh gases cone is now elevated. As the consumption of acetone occurs across a distance of a few camera pixels, the position of the net fluorescence reduction on the image can be precisely determined and laminar flame speeds can be accurately assessed.

4.2.2. Kerosene/air mixtures. In figure 12, the results of laminar flame speed measurements for Jet A-1 kerosene fuel with the kerosene-PLIF and OH-PLIF techniques are summarized. The average molecular formulation of Jet A-1 kerosene in the
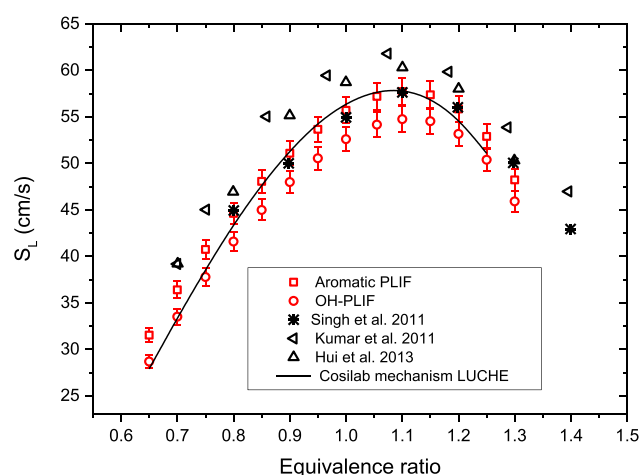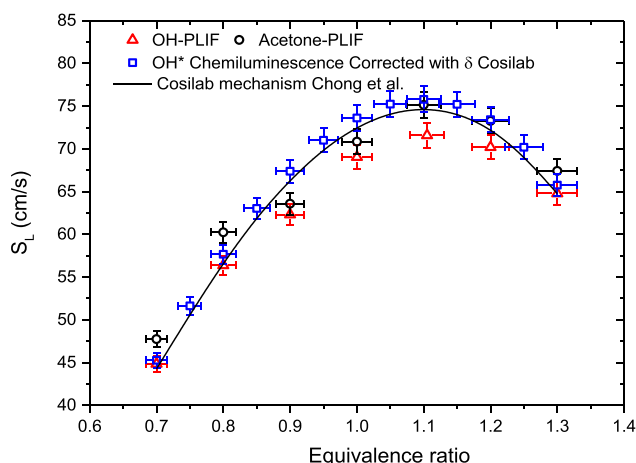

Figure 12. Laminar flame speeds determined from aromatics-PLIF and OH-PLIF images. Case of a Jet A-1/air mixture, $T = 400$ K, $P = 0.1$ MPa, $\varphi = 0.65$–1.3.

present study was considered as $C_{11.16}H_{20.82}$, with a molar mass of 154 g mol^{-1} [29]. The same trends are observed as in the case of acetone/air mixtures: the laminar flame speed deduced from the fuel-PLIF technique is slightly larger than the one acquired with the OH-PLIF technique. Note also that deviations in laminar flame speeds are less obvious on the lean and rich sides and maximal when the equivalence ratio approaches the stoichiometry. The maximum deviation at $\varphi = 1.0$ is about 5 cm s^{-1}.
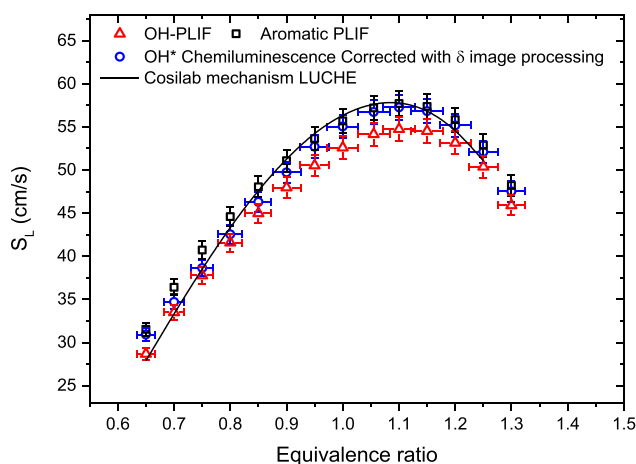
We compared our experimental results with the literature studying the laminar flame speeds of Jet A-1. For conditions of $T = 400$ K, there is a good agreement between the measurements reported by Hui *et al* [30], Singh *et al* [31] and Kumar *et al* [32] and our measurements for lean conditions, i.e. between 0.7 and 0.8. For $0.8 < \varphi < 1.1$, there is still a good agreement with the data of Hui *et al*. In contrast, significant deviations are noted with the data of Kumar *et al* [32], who used counter-flow flames and Singh *et al* [31], who used spherically expanding flames. Typically, the data of Kumar *et al* over-predict the measurements, while those of Singh *et al* under-predict our laminar flame speeds. For $\varphi > 1.2$, all the data referenced in the literature are systematically higher values.

4.3. Comparison between OH* chemiluminescence and PLIF

4.3.1. Acetone/air mixtures. In this section, a comparison of experimental results between the OH-PLIF, acetone-PLIF and OH* chemiluminescence techniques is conducted. Shown in figure 13 are the laminar flame speeds of acetone/air mixtures derived from these three optical measurement techniques. The experimental conditions are as follows: $T = 453$ K, $P = 0.1$ MPa and $\varphi = 0.7$–1.3. The laminar flame speeds deduced from the acetone-PLIF technique are in good accordance with those deduced from the OH* chemiluminescence images corrected by the flame thickness. Both of these two techniques give good agreement with simulation results performed using Chong *et al*'s [21] mechanism.
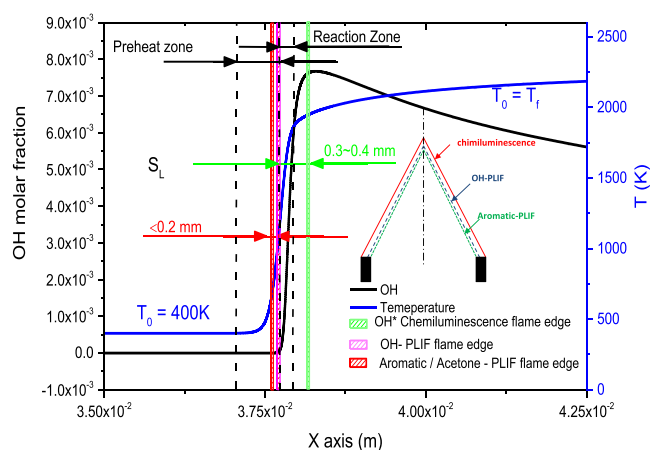
Figure 13. Laminar flame speed of acetone/N_2/O_2 mixtures measured by OH-PLIF, acetone-PLIF and OH* chemiluminescence with correction of the flame thickness. $T = 443$ K, $P = 0.1$ MPa, $\varphi = 0.7$–1.3.

Figure 15. Numerical simulation of one-dimensional laminar premixed flame. Temperature (blue curve) and OH (black curve) profiles for LUCHE surrogate/air mixture ($T = 400$ K, $P = 0.1$ MPa, $\varphi = 1.0$). The locations of the flame edges, measured using various measurement techniques, are also displayed.

molecule weight fuel/air mixtures, numerical simulation of the LUCHE surrogate/air flame was performed with Cosilab, using the LUCHE skeletal mechanism [22]. The calculation was performed at $T = 400$ K, $P = 0.1$ MPa and at an equivalence ratio of $\varphi = 1.0$. The flame sheet in figure 15 is expanded to reveal a preheat zone in which initiation reactions take place and a reaction zone in which intermediates are chemically produced and consumed (in particular OH radical). However, the distinction between both zones is difficult to establish experimentally. As shown in figure 15, the chemiluminescence imaging technique gives an OH* peak characteristic of the maximum temperature zone, and also therefore of the outer edge of the reaction zone. The gap between this location and the position of the outer edge of the preheat zone, i.e. the thermal flame thickness, is therefore quite significant. The possibility of getting a substantial bias for the laminar flame speed will then be inevitable if the outer edge of the reaction zone is employed. Looking now at the diagnostic performance of the OH-PLIF technique, it allows for the detection of the inner edge of the reaction zone when OH fluorescence becomes detectable (i.e. at a temperature of around 800 K). In such cases, the error on the laminar flame speed will be now greatly reduced because of the shorter gap between this new location and the outer edge of the preheat zone. With the fuel-PLIF technique, a visualization of the outer edge of the fresh gases will be obtained. As the fluorescence of the organic tracers decrease with increased temperature and at temperatures of around 800 K the fluorescence becomes to be undetectable [20], then theoretically, the outer edge delimiting the contour of the fluorescence signal of the organic tracer should correspond to a position quite similar to that for when OH-PLIF fluorescence begins to appear. However, the distance between these two contours are enlarged by the limitations of the camera dynamic. This limitation can, however, introduce considerable differences in the derivation of laminar flame speeds.

Figure 14. Laminar flame speeds determined from OH* chemiluminescence, aromatics-PLIF and OH-PLIF images. Case of a Jet A-1/air mixture, $T = 400$ K, $P = 0.1$ MPa, $\varphi = 0.65$–1.3.

4.3.2. Kerosene/air mixtures. Figure 14 presents the results of Jet A-1 kerosene derived by the OH* chemiluminescence, OH-PLIF and kerosene-PLIF techniques. The detailed kinetic mechanism of commercial Jet A-1 kerosene, a multicomponent mixture of thousands of hydrocarbons, is less unavailable and its skeletal mechanism is not precise enough to predict the flame thickness. When the chemiluminescence technique is applied, the flame thickness is estimated by the aforementioned image processing procedures. The same trends were observed as in the case of acetone/air mixtures: the laminar flame speed deduced from OH* chemiluminescence, corrected with flame thickness obtained via image processing, is slightly larger than that acquired with the OH-PLIF technique. On the other hand, the aromatic-PLIF technique gives laminar flame speeds similar to those obtained with OH* chemiluminescence.

In order to better understand the correspondence between different optical techniques and 1D flame structure for large

5. Conclusions

Measurements of laminar flame speed are performed for CH_4/air, acetone/air and kerosene/air mixtures using different optical diagnostic techniques, including the OH^* chemiluminescence, OH-PLIF and acetone/kerosene-PLIF techniques, based on a Bunsen flame approach. To summarize, it appears that the OH^* chemiluminescence imaging technique cannot directly derive the location of the outer edge of the preheat gases. To be in accordance with the definition of laminar flame speed, it is then necessary to make a correction regarding the position of the OH^* peak. For this purpose, to find the position of the outer edge, it is proposed to subtract the thermal flame thickness from the position measured with chemiluminescence imaging. As measuring this thermal flame thickness is challenging, these measurements were deduced from numerical digital calculations performed using a detailed kinetic mechanism. Of course, this method is only valid when the detailed kinetic mechanism of the fuel under study is available. On the contrary, the position measured from PLIF images were directly used for measuring the laminar flame speeds. Fuel-PLIF compared to OH^* chemiluminescence can directly determine the fresh gas edge and there is no need to correct the flame area by the flame thickness. However, one limitation of this diagnostic is its applicability, limited to the case of fluorescence fuels. In the case of optically transparent flues, the use of a tracer fuel seeded into the target fuel could be an alternative to visualize the fresh gas zone, but this will inevitably lead to a systematic bias of the resulting laminar flame speeds due to the modification of fuel consumption. Despite this, the fuel-PLIF technique compared to OH-PLIF and OH^* chemiluminescence technique is a better option to measure laminar flame speed of real aviation fuels. Besides real aviation fuels, the fuel-PLIF technique also provides an alternative solution for accurate laminar flame speed measurements targeting most of commercial fuels, such as gasoline and diesel fuels which exhibit the interesting features of strong UV absorption and thus large fluorescence emissions.

ORCID iDs

Yi Wu ● https://orcid.org/0000-0002-3255-2702

References

[1] Beeckmann J, Cai L and Pitsch H 2014 Experimental investigation of the laminar burning velocities of methanol, ethanol, n-propanol, and n-butanol at high pressure *Fuel* **117** 340–50

[2] Chen Z 2010 Effects of radiation and compression on propagating spherical flames of methane/air mixtures near the lean flammability limit *Combust. Flame* **157** 2267–76

[3] Battin-Leclerc F 2008 Detailed chemical kinetic models for the low-temperature combustion of hydrocarbons with application to gasoline and diesel fuel surrogates *Prog. Energy Combust. Sci.* **34** 440–98

[4] Andrews G E and Bradley D 1972 Determination of burning velocities: a critical review *Combust. Flame* **18** 133–53

[5] Dirrenberger P *et al* 2014 Laminar burning velocity of gasolines with addition of ethanol *Fuel* **115** 162–9

[6] Kumar K 2007 Global combustion response of practical hydrocarbon fuels: n-heptane, iso-octane, n-decane and ethylene *PhD Thesis* Case Western University

[7] Natarajan J, Lieuwen T and Seitzman J 2007 Laminar flame speeds of H2/CO mixtures: effect of CO2 dilution, preheat temperature, and pressure *Combust. Flame* **151** 104–19

[8] Wu Y, Modica V, Rossow B and Grisch F D R 2016 Effects of pressure and preheating temperature on the laminar flame speed of methane/air and acetone/air mixtures *Fuel* **185** 577–88

[9] Wang Z H, Weng W B, He Y, Li Z S and Cen K F 2015 Effect of H2/CO ratio and N2/CO2 dilution rate on laminar burning velocity of syngas investigated by direct measurement and simulation *Fuel* **141** 285–92

[10] Dominik E and Noel T C 2016 Simultaneous high-speed 3D flame front detection and tomographic PIV *Meas. Sci. Technol.* **27** 035303

[11] Fujisawa N and Nakashima K 2007 Simultaneous measurement of three-dimensional flame contour and velocity field for characterizing the flickering motion of a dilute hydrogen flame *Meas. Sci. Technol.* **18** 2103

[12] Gamba M, Clemens N T and Ezekoye O A 2013 Volumetric PIV and 2D OH PLIF imaging in the far-field of a low Reynolds number nonpremixed jet flame *Meas. Sci. Technol.* **24** 024003

[13] Nau P, Kruger J, Lackner A, Letzgus M and Brockhinke A 2012 On the quantification of OH^*, CH^*, and $C2^*$ chemiluminescence in flames *Appl. Phys.* B **107** 551–9

[14] Migliorini F, Maffi S, Iuliis S D and Zizak G 2014 Analysis of chemiluminescence measurements by grey-scale ICCD and colour digital cameras *Meas. Sci. Technol.* **25** 055202

[15] Gregory-Smith D G, Gilchrist A R and Senior P 1990 A combined system for measurements of high-speed flow by interferometry, schlieren and shadowgraph *Meas. Sci. Technol.* **1** 419

[16] Arndt C M, Gounder J D, Meier W and Aigner M 2012 Auto-ignition and flame stabilization of pulsed methane jets in a hot vitiated coflow studied with high-speed laser and imaging techniques *Appl. Phys.* B **108** 407–17

[17] Hanson R K, Seitzman J M and Paul P H 1990 Planar laser-fluorescence imaging of combustion gases *Appl. Phys.* B **50** 441–54

[18] Parrish S E and Zink R J 2013 Development and application of a high-speed planar laser-induced fluorescence imaging system to evaluate liquid and vapor phases of sprays from a multi-hole diesel fuel injector *Meas. Sci. Technol.* **24** 025402

[19] Koch J D and Hanson R K 2003 Temperature and excitation wavelength dependencies of 3-pentanone absorption and fluorescence for PLIF applications *Appl. Phys.* B **76** 319–24

[20] Orain M, Baranger P, Ledier C, Apeloig J and Grisch F 2014 Fluorescence spectroscopy of kerosene vapour at high temperatures and pressures: potential for gas turbines measurements *Appl. Phys.* B **116** 729–45

[21] Chong C T and Hochgreb S 2011 Measurements of laminar flame speeds of acetone/methane/air mixtures *Combust. Flame* **158** 490–500

[22] Luche J, Reuillon M, Boettner J-C and Cathonnet M 2004 Reduction of large detailed kinetic mechanisms: application to kerosene/air combustion *Combust. Sci. Technol.* **176** 1935–63

[23] Wu Y, Rossow B, Modica V, Yu X, Wu L and Grisch F 2017 Laminar flame speed of lignocellulosic biomass-derived oxygenates and blends of gasoline/oxygenates *Fuel* **202** 572–82

[24] Toulouzan J N L, Locquet J J, Allano D, Savary P and Darrigo R 1981 Abel's inversion of a cylindrical helium

plasma. Production of a stigmatic spectrograph using a vidicon detector *J. Opt.* **12** 369

[25] Mazas A N, Fiorina B, Lacoste D A and Schuller T 2011 Effects of water vapor addition on the laminar burning velocity of oxygen-enriched methane flames *Combust. Flame* **158** 2428–40

[26] Smith G P *et al* 1999 GRI-Mech homepage (http://www.me.berkeley.edu/gri_mech/) (Accessed: 04 November 2017)

[27] Beeckmann J *et al* 2013 Collaborative study for accurate measurements of laminar burning velocity *Proc. European Combustion Meeting (ECM)*

[28] Hu E, Li X, Chen Y, Cheng Y, Xie Y and Huang Z 2015 Laminar flame speeds and ignition delay times of methane-air mixture at elevated temperatrue and pressures *Fuel* **158** 1–10

[29] Vukadinovic V, Habisreuther P and Zarzalis N 2013 Influence of pressure and temperature on laminar burning velocity and Markstein number of kerosene Jet A-1: experimental and numerical study *Fuel* **111** 401–10

[30] Hui X and Sung C-J 2013 Laminar flame speeds of transportation-relevant hydrocarbons and jet fuels at elevated temperatures and pressures *Fuel* **109** 191–200

[31] Singh D, Nishiie T and Li Q 2011 Experimental and kinetic modeling study of the combustion of n-decane, Jet-A, and S-8 in laminar premixed flames *Combust. Sci. Technol.* **183** 1002–26

[32] Kumar K, Sung C-J and Hui X 2011 Laminar flame speeds and extinction limits of conventional and alternative jet fuels *Fuel* **90** 1004–11